Progress In Electromagnetics Research B, Vol. 25, 349–367, 2010

RADIOPHYSICAL AND DIELECTRIC PROPERTIES OF ORE MINERALS IN 12–145 GHZ FREQUENCY RANGE

V. V. Tikhonov and D. A. Boyarskii

Department of Remote Sensing of the Earth
Space Research Institute, Russian Academy of Sciences
Profsojuznaya, 84/32, Moscow 117997, Russia

O. N. Polyakova, A. L. Dzardanov, and G. N. Gol'tsman

Department of Physics
Moscow State Pedagogical University
M. Pirogovskaya, 29, Moscow, GSP-2, 119992, Russia

Abstract—The paper discusses a retrieval technique of complex permittivity of ore minerals in frequency ranges of 12–38 GHz and 77–145 GHz. The method is based on measuring frequency dependencies of transmissivity and reflectivity of plate-parallel mineral samples. In the 12–38 GHz range, the measurements were conducted using a panoramic standing wave ratio and attenuation meter. In the 77–145 GHz range, frequency dependencies of transmissivity and reflectivity were obtained using millimeter-band spectrometer with backward-wave oscillators. The real and imaginary parts of complex permittivity of a mineral were determined solving an equation system for frequency dependencies of transmissivity and reflectivity of an absorbing layer located between two dielectric media. In the course of the work, minerals that are primary ores in iron, zinc, copper and titanium mining were investigated: magnetite, hematite, sphalerite, chalcopyrite, pyrite, and ilmenite.

1. INTRODUCTION

Remote sensing studies of the Earth and the other planets have various applications in industry and sciences. Airborne and satellite remote sensing is widely employed in exploration and engineering geology:

Received 24 July 2010, Accepted 20 September 2010, Scheduled 23 September 2010
Corresponding author: V. V. Tikhonov (vtikhonov@asp.iki.rssi.ru).

mineral exploration, dam monitoring, etc. [1, 2]. Insufficient knowledge of dielectric properties of rockforming and ore minerals in the above frequency ranges poses a serious problem for further proliferation of the remote sensing methods. There is almost no data on dielectric properties of ore minerals in the microwave range in literature [3, 4].

At present, a variety of methods and techniques exist for the determination of complex permittivity of solid, liquid and bulk media in the microwave range. There are resonance, waveguide, quasi-optical and other methods [5, 6]. Each of them deals primarily with uniform and, as a rule, dielectric materials.

Investigation of dielectric properties of ore minerals in the microwave range is technically complicated due to high absorption of electromagnetic radiation of the media [7]. Complex permittivity cannot be measured directly. The real and imaginary parts of complex permittivity can be computed based on certain measurements and theory [8]. The measured parameters could be reflection and transmission coefficient, dielectric dissipation, Brewster angle, etc. [5, 6].

In the present work, complex permittivity of a substance in the given frequency range has been inferred from frequency dependencies of its reflectivity and transmissivity. We have investigated minerals that are primary ores in iron, zinc, copper and titanium mining.

2. MEASUREMENT TECHNIQUE

2.1. Parameters of Mineral Samples

For laboratory investigation the following mineral samples were prepared: Magnetite Fe_3O_4 (Fe — 72.4%), chalcopyrite $CuFeS_2$ (Cu — 34.6%, Fe — 30.5%), pyrite FeS_2 (Fe — 46.6%), hematite Fe_2O_3 (Fe — 70%), sphalerite ZnS (Zn — 67.1%), and ilmenite $FeTiO_3$ (Fe — 36.8%, Ti — 31.6%) [7]. These minerals are primary ores for iron (magnetite, hematite, ilmenite, pyrite), zinc (sphalerite) and titanium (ilmenite). All the minerals have relatively small effective resistivity in low frequencies (10^{-5}–$10^4\,\Omega\cdot$m) and are considered semiconductors [3]. Note, we could not obtain mono-mineral samples of the required size (~ 1 cm). Crystals of such dimensions are scarce in nature and can mostly be encountered in museums [9]. The samples under study were intergrowth structures of several crystals of a mineral. The number of pores (fine cavities) and non-ore impurities (quartz, feldspar and plagioclase) did not exceed 10%.

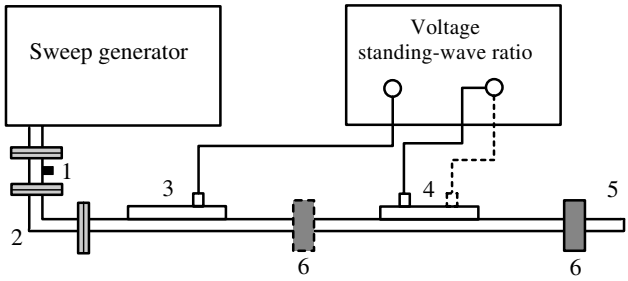

Figure 1. Design of the panoramic standing wave ratio and attenuation meter. 1 — attenuator, 2 — waveguide junction, 3 — forward couple, 4 — reverse couple, 5 — matched load, 6 — sample. Dash and dot: position of the items for attenuation measurement.

2.2. The 12–38 GHz Frequency Range

Frequency dependencies of reflectivity $R(f)$ and transmissivity $T(f)$ of plate-parallel mineral samples in the frequency range of 12–38 GHz were measured with a panoramic standing wave ratio and attenuation meter [5]: R2-67 (12–17 GHz), R2-66 (17–26 GHz), R2-65 (25–38 GHz). The samples were manufactured for waveguide cell N 1 with dimensions of 11×5.5 mm (17–26 GHz) and waveguide cell N 2 with dimensions of 16×8 mm (12–17 GHz). For the frequency range of 25–38 GHz, a waveguide junction was used connecting cell N 1 and a waveguide with dimensions of 8×3.6 mm. The design of the experimental set for standing wave ratio and attenuation measurement is presented in Fig. 1.

Panoramic meters are based on separation and direct detection of the incident and reflected wave signals. When measuring reflection (Fig. 1), the signal proportional to the voltage amplitude of the wave incident on the study sample is intercepted by the forward couple. The signal reflected from the sample is intercepted by the reverse couple. A scaling device shows directly the standing wave ratio based on voltage ρ. Reflectivity R is defined as [5]:

$$R = \left(\frac{\rho - 1}{\rho + 1}\right)^2. \tag{1}$$

When measuring transmission (Fig. 1), the attenuation of a signal transmitted through a sample is registered in dB, based on which the transmissivity T is then computed [5]. In the experiment, we were able to measure the value of T to the order of 10^{-4}. The errors of R and T measurements did not exceed 5%.

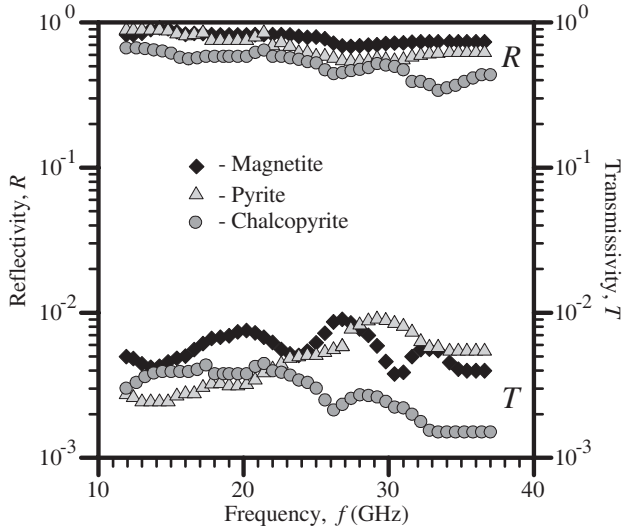

Figure 2. Spectral dependencies $R(f)$ and $T(f)$ in the 12–38 GHz frequency range for three mineral samples with thicknesses: magnetite — 0.55 cm, pyrite — 0.48 cm, chalcopyrite — 0.57 cm.

In the course of the experiment, dependencies of $R(f)$ and $T(f)$ were obtained for three minerals: chalcopyrite, pyrite and magnetite (Fig. 2).

No measurements of reflectivity and transmissivity of other minerals in the 12–38 GHz frequency range were performed. Because of extreme brittleness of the minerals [7], it was impossible to prepare samples suitable for the waveguide cell dimensions.

2.3. The 77–145 GHz Frequency Range

Dependencies $R(f)$ and $T(f)$ of mineral samples in the 77–145 GHz frequency range were measured with a millimeter-band spectrometer based on backward-wave oscillators (millimeter BWO — spectrometer). The spectrometer comprised a generator, a measurement quasi-optical path and a receiving unit (Fig. 3).

The following sources of monochromatic electromagnetic radiation were used: generator RG4-14 (BWO-71) for frequencies 77–119 GHz, generator G4-161 (BWO-76) for frequencies 126–145 GHz.

The measuring quasi-optical path of the spectrometer was designed on the basis of quasi-optical waveguides. The waveguides provided single-mode propagation of an electromagnetic wave due to absorption of other types of waves by a lossy dielectric.

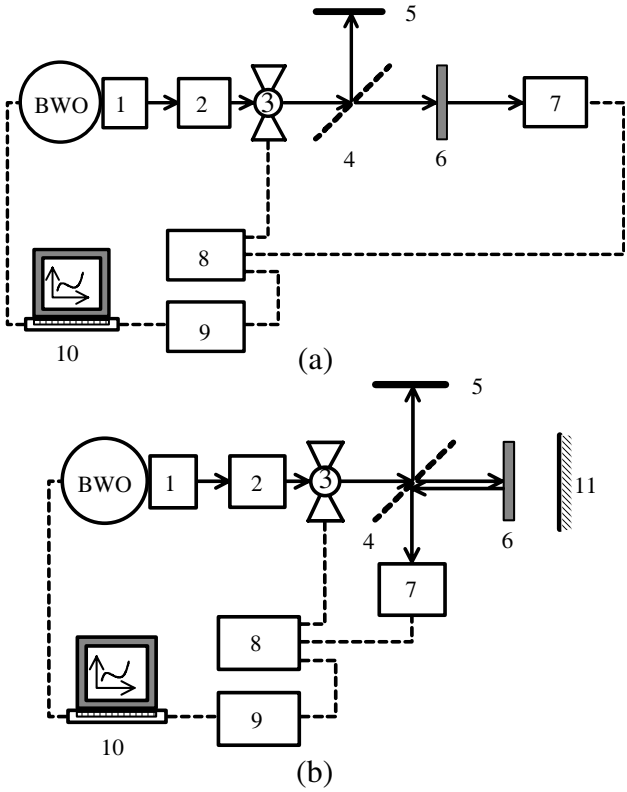

Figure 3. Schematic diagram of the millimeter BWO — spectrometer: (a) measuring $T(f)$, (b) measuring $R(f)$. 1 — horn/waveguide-to-quasi-optical adapter, 2 — attenuator, 3 — modulator, 4 — beam splitter, 5 — microwave absorber, 6 — study sample, 7 — optophone, 8 —- synchronous detector, 9 — digital voltmeter, 10 — computer, 11 — mirror.

The receiving unit comprised a receiver — Golay cell (receiving element of an optophone), a synchronous detector and a digital voltmeter Agilent 34401 A.

Monochromatic radiation outcoming from the BWO entered the measurement path via the horn (77–119 GHz) or the waveguide-to-quasi-optical adapter (126–145 GHz). The electromagnetic radiation was amplitude-modulated by means of a mechanical modulator with a frequency of 12.5 Hz, and then transferred via the quasi-optical path to the receiving unit.

When measuring transmission spectrum, the sample was fixed so that the incident radiation was normal to the sample surface, and the

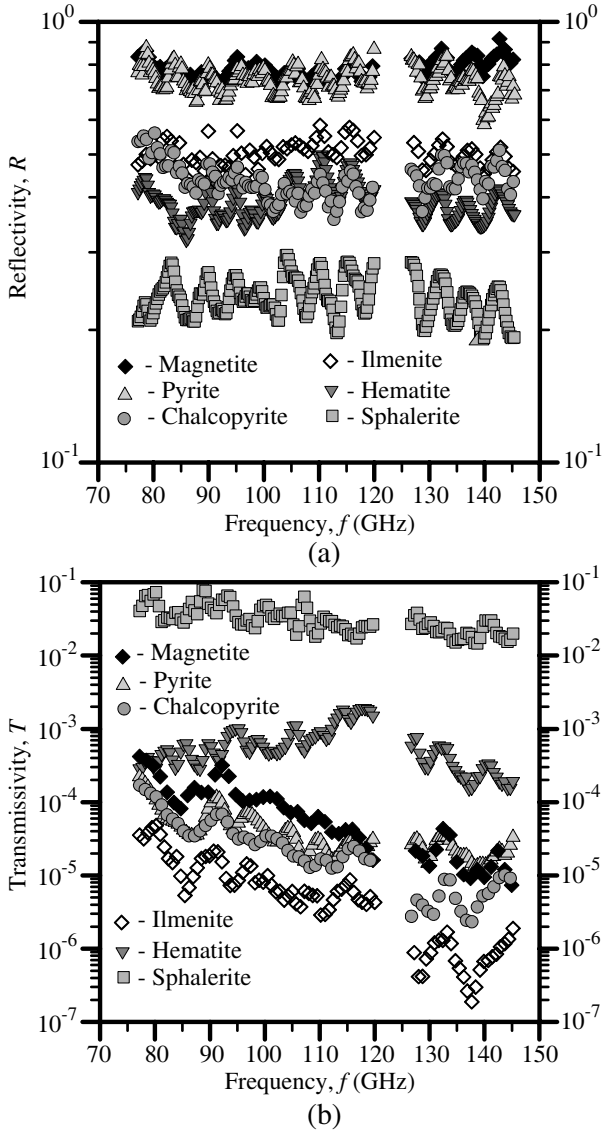

Figure 4. Spectral dependencies (a) $R(f)$ and (b) $T(f)$ in the 77–145 GHz frequency range for samples of six minerals. Thicknesses of the samples are: magnetite — 1.283 cm, pyrite — 1.275 cm, chalcopyrite — 1.33 cm, ilmenite — 2.01 cm, hematite — 1.98 cm, sphalerite — 1.963 cm.

sample covered completely the aperture of the waveguide (Fig. 3(a)). Electromagnetic radiation fell onto a 0.03-mm-thick beam splitter. In the 77–145 GHz frequency range, the plate transmissivity was 50%. Part of the radiation was reflected from the plate to follow the second path of the experimental set. An absorber was placed there in order to avoid secondary resonances due to re-reflection at the beam splitter.

Before the measurement, the experimental set was calibrated in the absence of the study sample. The power of microwave radiation incident onto the receiver was decreased by a calibrated polarization attenuator capable to attenuate the signal by 30 dB.

The transmission spectrum $T(f)$ was measured in two stages. First, the frequency dependence $P_1(f)$ of the signal power without the sample in the measurement path was registered; second, the signal power $P_2(f)$ in the presence of the sample in the measurement path was obtained. The absolute value of transmissivity of the sample was computed dividing one array of numbers by the other:

$$T(f) = \frac{P_2(f)}{P_1(f)}. \tag{2}$$

In the experiment, the measurements of were achieved to the order of 10^{-7}.

The reflection spectrum $R(f)$ also was defined in two stages. First, the power frequency dependence of a signal reflected from the calibration mirror $P_3(f)$ held in place of the sample was obtained (Fig. 3(b)). The signal was reflected from the beam splitter and registered by the receiver. Then the power frequency dependence of a signal reflected from the sample (in place of the calibration mirror) $P_4(f)$ was measured. The absolute value of reflectivity of the sample was computed dividing one array of numbers by the other:

$$R(f) = \frac{P_4(f)}{P_3(f)}. \tag{3}$$

The measurement error was up to 3%. Results of $R(f)$ and $T(f)$ measurements for all mineral study samples are presented in Fig. 4.

3. CALCULATION OF THE DIELECTRIC PROPERTIES

For the purpose of determining the real ε' and imaginary ε'' parts of complex permittivity $\varepsilon = \varepsilon' + i\varepsilon''$ of the minerals from spectral dependencies $R(f)$ and $T(f)$, the following problem was considered (Fig. 5).

Flat electromagnetic wave with intensity I_0 illuminates a plate-parallel layer of substance (medium 2) placed in vacuum (medium 1)

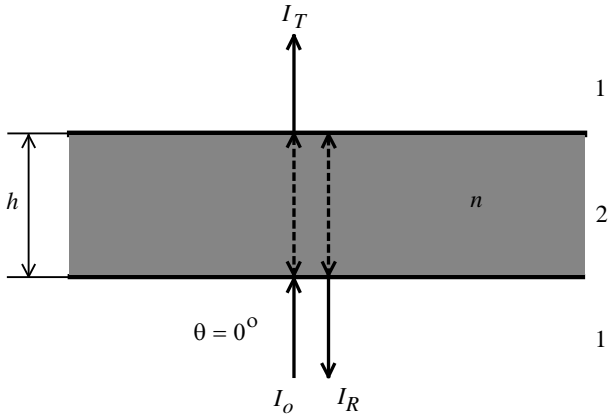

Figure 5. Outline of the problem.

at an angle $\theta = 0^o$. The layer has thickness h and complex index of refraction $n = n' + in''$. Intensities I_R and I_T of the radiations reflected from the layer and transmitted through it, respectively, taking into account multiple reflections at the layer boundaries, are determined by the following relationships [10]:

$$I_R = RI_0, \quad I_T = TI_0. \tag{4}$$

R and T are reflectivity and transmissivity related to reflection coefficient r and transmission coefficient t as follows [10]:

$$R = |r|^2, \quad T = |t|^2, \quad r = \frac{r_{12} - r_{12}e^{2i\beta}}{1 - r_{12}^2 e^{2i\beta}}, \quad t = \frac{(1 - r_{12}^2)e^{i\beta}}{1 - r_{12}^2 e^{2i\beta}}, \tag{5}$$

where $r_{12} = \frac{1-n}{1+n}$ is vacuum-medium boundary reflection coefficient, $\beta = \frac{2\pi}{\lambda} nh$, λ is radiation wavelength. The real and imaginary parts of complex permittivity are related to the real and imaginary parts of complex refractive index as:

$$\varepsilon' = n'^2 - n''^2, \quad \varepsilon'' = 2n'n''. \tag{6}$$

In order to determine n' and n'' of a substance, it is necessary to solve the equation system (5). The system does not allow analytical solution and has to be approached with numerical methods. Each range where $R(f)$ and $T(f)$ dependencies of the minerals were obtained (12–38 GHz and 77–145 GHz), was divided into equal frequency intervals of width Δf. The real and imaginary parts of complex refractive index of a mineral in the frequency range Δf are assumed to be constant. For each interval Δf, values of n' and n''

were defined minimizing the criterion function $F(n', n'')$. The criterion function

$$F(n',n'')=\frac{1}{M}\sum_{k=1}^{M}\left(\frac{(R_t(n',n'',f_k)-R_e(f_k))^2}{R_e^2(f_k)}+\frac{(T_t(n',n'',f_k)-T_e(f_k))^2}{T_e^2(f_k)}\right) \quad (7)$$

is the sum of quadrates of coefficient of variation of theoretical dependences reflectivity and transmissivity in the Δf interval. In expression (7): f_k is radiation frequency in interval Δf; $R_t(n', n'', f_k)$ and $T_t(n', n'', f_k)$ is theoretical value of R and T calculated based on (5) for the given optimization parameters n' and n'' at radiation frequency f_k; $R_e(f_k)$ and $T_e(f_k)$ is experimental value of R and T at the same radiation frequency; M is the number of experimental points in frequency interval Δf.

Minimization of the criterion function was achieved by Rosenbrock method [11]. Rosenbrock method was successfully employed by the authors when determining structural parameters of dry sandstones [12, 13].

The retrieved n' and n'' were approximated by smooth functions of radiation frequency. Below, the resulting approximation expressions for n' and n'' are presented for all the study minerals: magnetite, range 12–145 GHz —

$$\begin{aligned} n' &= 32.02744215 - 0.5259548602f - 0.06491391718f^2 \\ &\quad + 3.608474987\times10^{-3}f^3 - 7.125902056\times10^{-5}f^4 \\ &\quad + 6.751320507\times10^{-7}f^5 - 3.113051295\times10^{-9}f^6 \\ &\quad + 5.632545142\times10^{-12}f^7, \\ n'' &= 2.520151324 - 0.3127286757f + 0.01875754576f^2 \\ &\quad - 5.916173864\times10^{-4}f^3 + 1.067064015\times10^{-5}f^4 \\ &\quad - 1.144566958\times10^{-7}f^5 + 7.234628417\times10^{-10}f^6 \\ &\quad - 2.491158837\times10^{-12}f^7 + 3.606967497\times10^{-15}f^8; \end{aligned} \quad (8)$$

pyrite, range 12–145 GHz —

$$\begin{aligned} n' &= 45.10123824 + 0.4750837566f - 0.2770431487f^2 \\ &\quad + 1.360410159\times10^{-2}f^3 - 2.920310577\times10^{-4}f^4 \\ &\quad + 3.327239518\times10^{-6}f^5 - 2.093060363\times10^{-8}f^6 \\ &\quad + 6.862839841\times10^{-11}f^7 - 9.151452873\times10^{-14}f^8, \end{aligned} \quad (9)$$

$$\begin{aligned} n'' &= 0.7031046195 + 1.990480306\times10^{-2}f \\ &\quad - 1.619627954\times10^{-3}f^2 + 3.351891491\times10^{-5}f^3 \\ &\quad - 3.167624788\times10^{-7}f^4 + 1.430090796\times10^{-9}f^5 \\ &\quad - 2.501858921\times10^{-12}f^6; \end{aligned}$$

chalcopyrite, range 12–145 GHz —

$$\begin{aligned} n' &= 30.7418328 - 4.336389741f + 0.3595593963f^2 \\ &\quad - 1.675195689 \times 10^{-2} f^3 + 4.558620163 \times 10^{-4} f^4 \\ &\quad - 7.481423268 \times 10^{-6} f^5 + 7.497642831 \times 10^{-8} f^6 \\ &\quad - 4.489031854 \times 10^{-10} f^7 + 1.475466346 \times 10^{-12} f^8 \\ &\quad - 2.048994751 \times 10^{-15} f^9, \\ n'' &= 4.228240003 - 0.4926839851f + 2.904899281 \times 10^{-2} f^2 \\ &\quad - 9.16536036 \times 10^{-4} f^3 + 1.661034607 \times 10^{-5} f^4 \\ &\quad - 1.791686078 \times 10^{-7} f^5 + 1.138378562 \times 10^{-9} f^6 \\ &\quad - 3.936338708 \times 10^{-12} f^7 + 5.715979178 \times 10^{-15} f^8. \end{aligned} \tag{10}$$

sphalerite, range 77–145 GHz —

$$\begin{aligned} n' &= 1.135383285 + 3.192460104 \times 10^{-2} f \\ &\quad - 1.448182453 \times 10^{-4} f^2, \\ n'' &= 5.678088171 \times 10^{-2} - 3.129785173 \times 10^{-4} f \\ &\quad + 8.396955542 \times 10^{-7} f^2; \end{aligned} \tag{11}$$

ilmenite, range 77–145 GHz —

$$\begin{aligned} n' &= -0.7877085347 + 0.1219783154f - 5.409869773 \times 10^{-4} f^2, \\ n'' &= 0.2611383566 - 2.181707959 \times 10^{-3} f + 7.895999332 \times 10^{-6} f^2; \end{aligned} \tag{12}$$

hematite, range 77–145 GHz —

$$\begin{aligned} n' &= 272.3284042 - 9.972816121f + 0.1367914484f^2 \\ &\quad - 8.20183364 \times 10^{-4} f^3 + 1.815397425 \times 10^{-6} f^4, \\ n'' &= -2.659658611 + 0.1073701638f - 1.511691203 \times 10^{-3} f^2 \\ &\quad + 9.125208162 \times 10^{-6} f^3 - 2.009006668 \times 10^{-8} f^4; \end{aligned} \tag{13}$$

In (8)–(13), f is radiation frequency in GHz.

The real ε' and imaginary ε'' parts of complex permittivity of the minerals are inferred from (6) with n' and n'' taken from (8)–(13). The suggested approximation expressions can be used for computing n' and n'' or ε' and ε'' of the minerals in the corresponding frequency ranges.

Figure 6 presents values of n' and n'' of the study minerals obtained solving system (5) and their approximation dependencies. For clarity, results for only 4 minerals are shown.

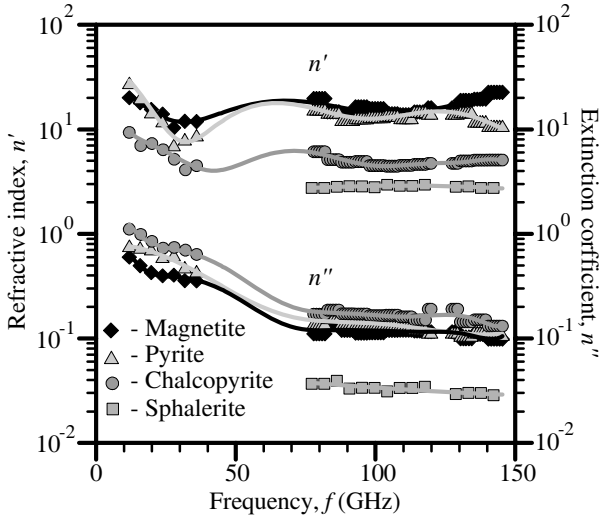

Figure 6. Frequency dependencies n' and n'' of the minerals. Symbols indicate values obtained by the numerical algorithm, solid lines are approximations of the values.

4. DISCUSSION OF THE RESULTS

In order to validate the obtained results, the n' and n'' approximations (8)–(13) were used to calculate R and T of the samples.

Calculation results for the 12–38 GHz frequency range are shown in Fig. 7. It is obvious from the figure, that the calculated frequency dependencies of n' and n'' of the minerals are in good agreement with the experimental data.

Comparison of the experimental and calculated $R(f)$ and $T(f)$ dependencies in the 77–145 GHz frequency range for four minerals are presented in Fig. 8. One can see that the calculations do agree with the experimental values. However, the former are smooth curves (except for sphalerite), while the latter have a pronounced oscillating shape.

Discrepancies between the calculated frequency dependencies $R(f)$ and $T(f)$ and experimental results are due to the fact that the study samples were not monominerals but intergrowths of ore mineral crystals divided by thin layers (≤ 1 mm) of barren minerals. Schematics of such a medium is shown in Fig. 9: light regions indicate ore mineral crystals, dark filaments are fine-grained fractions of barren minerals.

At first view, the medium can be represented as a multi-layer structure where an ore mineral is interlayered with very thin bands

of a barren mineral. Absorption of an ore mineral layer is high, that is why the reflectivity of the sample is determined by reflection at the boundary of the first two layers of the structure, the ore and the barren ones. The input of the other boundaries of the structure into reflectivity is negligible. The transmissivity of the medium is determined by radiation transition through all the layers and re-reflection at the boundary between the last two layers. Re-reflection at the other layer boundaries has no considerable impact on T because of high absorption of the ore mineral. Therefore, the calculation of R and T can be achieved solving the problem of radiation reflection and transmission through a three-layer medium shown in Fig. 10. In the figure, media 1 and 5 are vacuum with refractive indices $n_1 = n_5 = 1$; media 2 and 4 are ore mineral layers with thicknesses h_2 and h_4 and complex refractive indices $n_2 = n_4$; medium 3 is barren mineral layer with thickness h_3 and complex refractive index n_3; total thickness of the sample is $h = h_2 + h_3 + h_4$.

Figure 10(a) shows a diagram for calculating reflectivity of the study samples. Here, medium 4 is a subsequent for all ore and barren mineral layers lying behind layers 1 and 2. Figure 10(b) shows a diagram for calculating transmissivity of the study samples. Here,

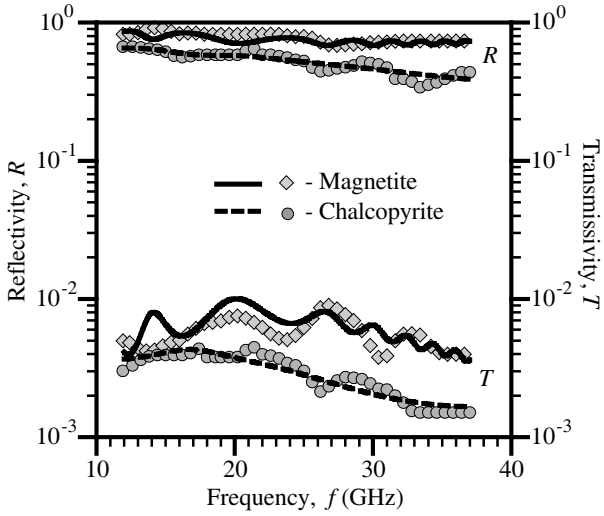

Figure 7. Frequency dependencies $R(f)$ and $T(f)$ in the 12–38 GHz frequency range for samples of two minerals. Symbols indicate experimental data, solid lines — calculations. Thicknesses of the samples are: magnetite — 0.55 cm, chalcopyrite — 0.57 cm.

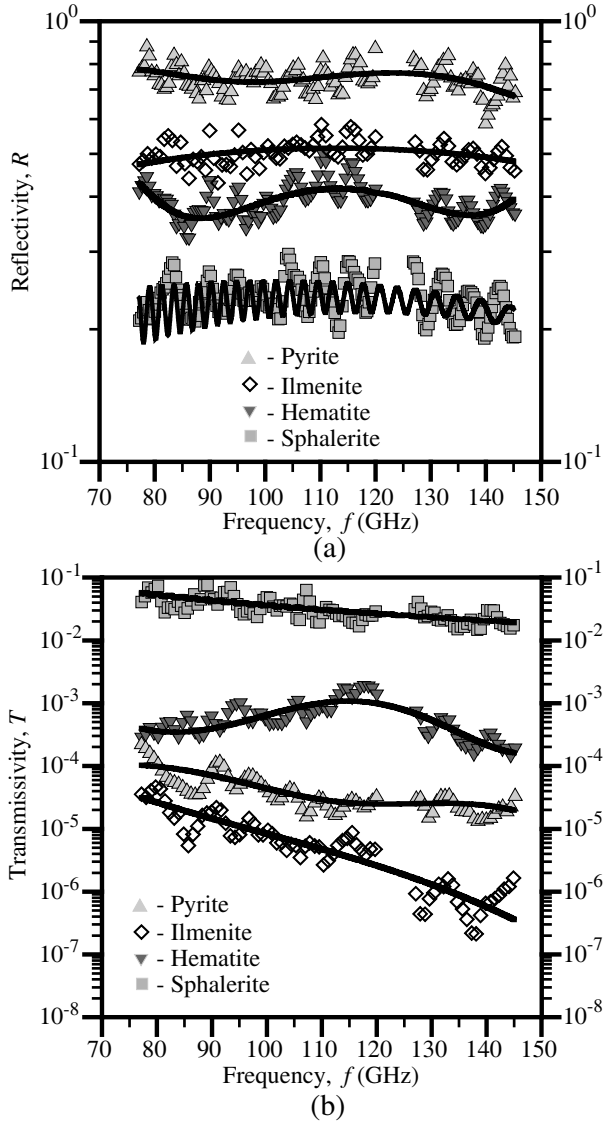

Figure 8. Frequency dependencies (a) $R(f)$ and (b) $T(f)$ in the 77–145 GHz frequency range for samples of four minerals. Symbols indicate experimental data, solid lines — calculations. Thicknesses of the samples are: pyrite — 1.275 cm, ilmenite — 2.01 cm, hematite — 1.98 cm, sphalerite — 1.963 cm.

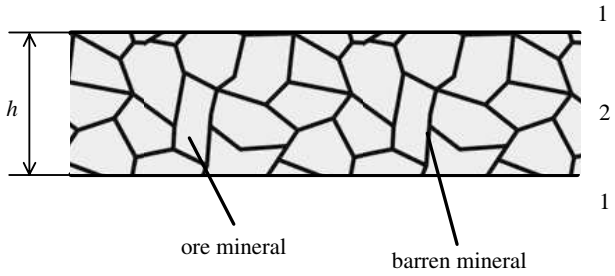

Figure 9. Schematics of the study samples.

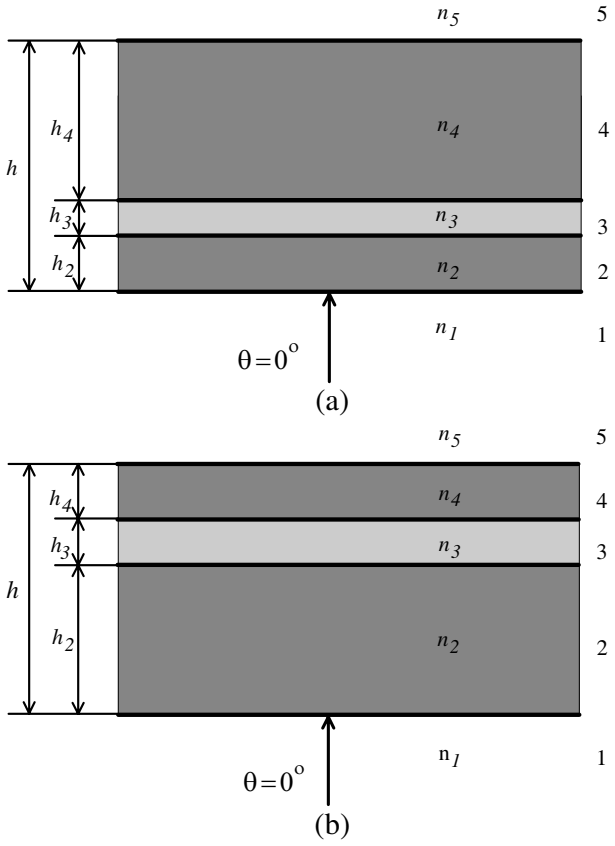

Figure 10. Calculation diagram for (a) R and (b) T.

medium 2 is a substitute for all ore and barren mineral layers lying above the next to the last and the last layers (3 and 4).

Reflectivity R and transmissivity T of a multiplayer plate-parallel medium in vacuum in conditions of an incident radiation at angle $\theta = 0^\circ$ are determined from the following expressions [10]:

$$\begin{aligned} R &= |r|^2, \quad r = \frac{M_{11} + M_{12} - M_{21} - M_{22}}{M_{11} + M_{12} + M_{21} + M_{22}}; \\ T &= |t|^2, \quad t = \frac{2}{M_{11} + M_{12} + M_{21} + M_{22}}; \end{aligned} \tag{14}$$

where r is reflection coefficient of the stratified medium; t is transmission coefficient of the stratified medium; $M_{11}, M_{12}, M_{21}, M_{22}$ are elements of characteristic matrix of the stratified medium. Characteristic matrix of a stratified medium $M(h)$ is determined as a product of characteristic matrices of each layer [10]. In our case:

$$M(h) = M_2(h_2)M_3(h_3)M_4(h_4) = \begin{bmatrix} M_{11} & M_{12} \\ M_{21} & M_{22} \end{bmatrix}, \tag{15}$$

where $M_2(h_2), M_3(h_3)$ and $M_4(h_4)$ are characteristic matrices of the corresponding layers. Characteristic matrix of a layer in our case is defined as [10]:

$$M_k(h_k) = \begin{bmatrix} \cos\beta_k & \frac{-i}{n_k}\sin\beta_k \\ -in_k\sin\beta_k & \cos\beta_k \end{bmatrix} \tag{16}$$

where $\beta_k = \frac{2\pi}{\lambda} n_k h_k$, λ is radiation wavelength, n_k and h_k are the layers complex refractive index and thickness, k is number of the layer (Fig. 10). Considering (16), let us obtain from (15) elements of characteristic matrix of a three-layer medium shown in Fig. 10. After introducing the obtained $M_{11}, M_{12}, M_{21}, M_{22}$ into (14), we infer expressions for reflection coefficient r_3 and transmission coefficient t_3 of the three-layer medium:

$$\begin{aligned} r_3 \;=\; & \Big(r_{12} + r_{23}e^{2i\beta_2} + r_{34}e^{2i(\beta_2+\beta_3)} + r_{45}e^{2i(\beta_2+\beta_3+\beta_4)} \\ & + r_{12}r_{23}r_{34}e^{2i\beta_3} + r_{12}r_{23}r_{45}e^{2i(\beta_3+\beta_4)} + r_{12}r_{34}r_{45}e^{2i\beta_4} \\ & + r_{23}r_{34}r_{45}e^{2i(\beta_2+\beta_4)}\Big) \\ & \times \Big(1 + r_{12}r_{23}e^{2i\beta_2} + r_{23}r_{34}e^{2i\beta_3} + r_{34}r_{45}e^{2i\beta_4} \\ & + r_{12}r_{34}e^{2i(\beta_2+\beta_3)} + r_{23}r_{45}e^{2i(\beta_3+\beta_4)} \\ & + r_{12}r_{23}r_{34}r_{45}e^{2i(\beta_2+\beta_4)} + r_{12}r_{45}e^{2i(\beta_2+\beta_3+\beta_4)}\Big)^{-1}, \end{aligned} \tag{17}$$

$$t_3 = \left(t_{12}t_{23}t_{34}t_{45}e^{i(\beta_2+\beta_3+\beta_4)}\right) \times\Big(1+r_{12}r_{23}e^{2i\beta_2}+r_{23}r_{34}e^{2i\beta_3}+r_{34}r_{45}e^{2i\beta_4} +r_{12}r_{34}e^{2i(\beta_2+\beta_3)}+r_{23}r_{45}e^{2i(\beta_3+\beta_4)} +r_{12}r_{23}r_{34}r_{45}e^{2i(\beta_2+\beta_4)}+r_{12}r_{45}e^{2i(\beta_2+\beta_3+\beta_4)}\Big)^{-1}, \quad (18)$$

where $r_{k,k+1} = \frac{n_k - n_{k+1}}{n_k + n_{k+1}}$ is reflection coefficient at the boundary between media k and $k+1$, $t_{k,k+1} = \frac{2n_k}{n_k+n_{k+1}}$ is transmission coefficient of the boundary between media k and $k+1$, $k = 1, 2, 3, 4$.

Expressions (17) and (18) were used for calculating R and T of the mineral study samples. Values of n' and n'' of the minerals were defined from (8)–(13). For each layer, its thickness (h_2, h_3, h_4) was chosen arbitrarily within a reasonable range [7]. Because dielectric characteristics of most barren minerals are similar [3, 4, 7], we chose quartz to play the role of a barren mineral since its n' and n'' are well-known in a wide frequency range [3, 4, 7, 14]. The samples' reflectivity were obtained from the diagram in Fig. 10(a), and transmissivity from the diagram in Fig. 10(b). Calculations were made for all mineral samples. Comparison of the calculated dependencies $R(f)$ and $T(f)$ and the experimental data in the 77–145 GHz showed a good agreement.

Figure 11 presents comparison results between the $R(f)$ and $T(f)$ frequency dependencies calculated based on (17) and (18), and the experimental data for three minerals. The calculation of R was performed given the following sample parameters: pyrite — $h_2 = 0.25$ cm, $h_3 = 0.02$ cm, $h_4 = 1.005$ cm; hematite — $h_2 = 0.46$ cm, $h_3 = 0.01$ cm, $h_4 = 1.51$ cm; sphalerite — $h_2 = 0.74$ cm, $h_3 = 0.15$ cm, $h_4 = 1.073$ cm. The calculation of T was performed given the following sample parameters: pyrite — $h_2 = 1.02$ cm, $h_3 = 0.008$ cm, $h_4 = 0.147$ cm; hematite — $h_2 = 1.64$ cm, $h_3 = 0.11$ cm, $h_4 = 0.23$ cm; sphalerite — $h_2 = 0.74$ cm, $h_3 = 0.15$ cm, $h_4 = 1.073$ cm. The figure demonstrates a good agreement between the calculated dependencies and experimental data.

Therefore, the oscillating shape of experimental frequency dependencies $R(f)$ and $T(f)$ in the 77–145 GHz range is linked with structural non-uniformity of the study samples, the presence of internal media boundaries. Expressions (5) are obtained for a structurally uniform medium. As all the samples (except sphalerite) highly absorb radiation and their thickness $h \gg \lambda$, radiation re-reflection at the opposite boundary of a sample has almost no effect on R and T. That is why in the 77–145 GHz range, the calculated dependencies $R(f)$ and

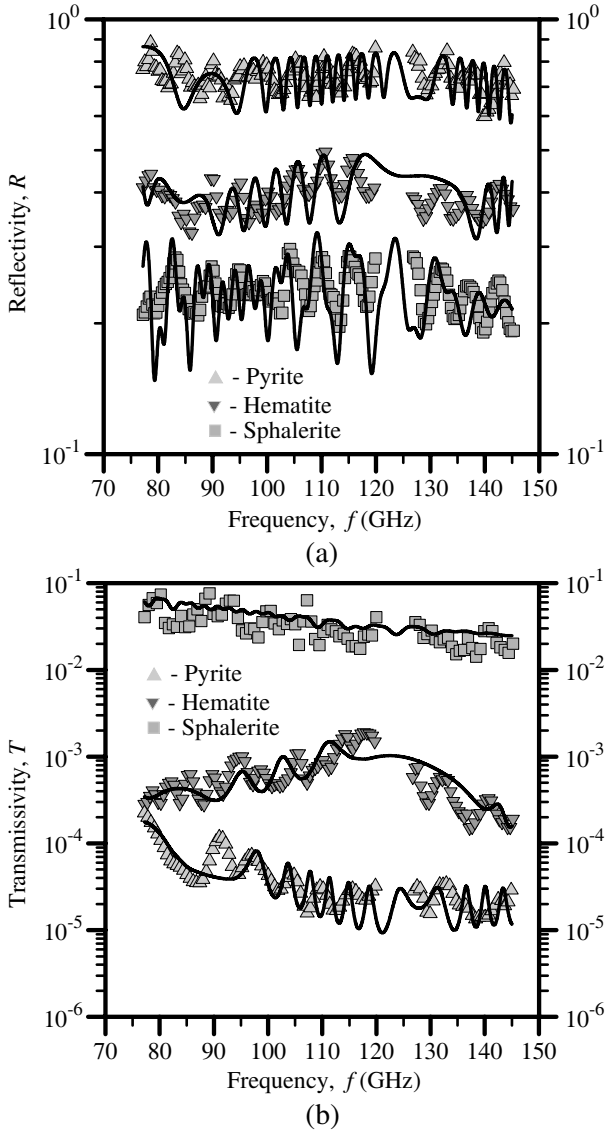

Figure 11. Frequency dependencies (a) $R(f)$ and (b) $T(f)$ in the 77–145 GHz range for three mineral samples. Symbols indicate experimental data, curves are calculations based on (a) (17) and (b) (18). Sample thicknesses are: pyrite — 1.275 cm, hematite — 1.98 cm, sphalerite — 1.963 cm.

$T(f)$ deduced from (5) have the shape of smooth curves (Fig. 8).

In the 12–38 GHz range, the samples' thickness is $h < \lambda$, and the thickness of barren mineral layers is $h_3 \ll \lambda$. In this range, the samples can be assumed uniform, and the calculation of R and T based on (5) yields almost the same results as the experiment (Fig. 7).

The problem diagram presented in Fig. 10 is an approximation of the natural sample structure (Fig. 9). In the samples, the thicknesses of ore and barren mineral layers are not even and the layers have ruptures (Fig. 9). Moreover, some boundaries between media within a sample may be unparallel to the external boundaries. This explains the discrepancies between theoretical and experimental frequency dependencies $R(f)$ and $T(f)$ (Figs. 7 and 11).

It can be easily shown that if $h_3 \to 0$ (Fig. 10) expressions (17) and (18) are transformed into equations (5). As barren mineral content in the samples did not exceed 10%, and $h_3 \ll h$, the obtained approximations of frequency dependencies n' and n'' for ore minerals (expressions (8)–(13)) can be considered highly reliable.

5. CONCLUSION

Approximation expressions for dielectric properties of a number of ore minerals in the 12–145 GHz frequency range are obtained. These expressions can be used in radiophysical studies of minerals and rocks, as well as Earth and planets remote sensing applications. The investigations performed and results obtained have proved validity of the developed technique for the determination of dielectric properties of ore minerals in the microwave range.

ACKNOWLEDGMENT

The authors express sincere gratitude to "TECHNOROS" and "RADOS" companies (Krasnoyarsk) for the mineral samples they provided. Work is executed at support Russian Fund of Basic Researches (project 10-05-00037).

REFERENCES

1. Rees, W. G., *Physical Principles of Remote Sensing*, Cambridge University Press, 2001.
2. Chandra, A. M. and S. K. Ghosh, *Remote Sensing and Geographical Information System*, Narosa Publishing House, 2006.

3. *Handbook of Physical Constants*, editor S. P. Clark, Jr., Yale University, New Haven, Connecticut, The Geol. Soc. of America, Inc. Memoir 97, 1966.
4. *Mineral Physics and Crystallography: a Handbook of Physical Constants*, editor J. A. Thomas, The American Geophysical Union, 1995.
5. Harvey, A. F., *Microwave Engineering*, Academic Press, 1963.
6. *Measurement, Instrumentation, and Sensors Handbook*, Editor-in-Chief J. G. Webster, CRC Press LLC, 1999.
7. Battey, M. H. and A. Pring, *Mineralogy for Students*, Longman, 1997.
8. Bohren, C. F. and D. R. Huffman, *Absorption and Scattering of Light by Small Particles*, Wiley-Interscience, New York, 1983.
9. Korbel, P. and M. Novak, *The Complete Encyclopedia of Minerals*, Grange Books Plc, Kent, UK, 2001.
10. Born, V. and E. Wolf, *Principles of Optics*, Pergamon, Oxford, 1964.
11. Himmelblau, D. M., *Applied Nonlinear Programming*, McGraw-Hill Book Company, Austin, Texas, 1972.
12. Boyarskii, D. A., et al., "On a possibility to determine microstructural parameters of oil-bearing layer from radiophysical measurements data," *J. of Communications Technology and Electronics*, Vol. 41, No. 5, 408–414, 1996.
13. Boyarskii, D. A., "Method of retrieval of media structural parameters from frequency dependence of transmission coefficient," *Proceeding of International Geoscience and Remote Sensing Symposium (IGARSS'96)*, Vol. 2, 1349–1351, Lincoln, Nebraska USA, May 27–31, 1996.
14. Clark, R. N., *Spectroscopy of Rocks and Minerals, and Principles of Spectroscopy*, John Wiley and Sons, Inc, New York, 1999.